

ENGINEERING

Life cycle energy use and environmental implications of high-performance perovskite tandem solar cells

Xueyu Tian¹, Samuel D. Stranks^{2,3}, Fengqi You^{1,4,5*}

A promising route to widespread deployment of photovoltaics is to harness inexpensive, highly-efficient tandems. We perform holistic life cycle assessments on the energy payback time, carbon footprint, and environmental impact scores for perovskite-silicon and perovskite-perovskite tandems benchmarked against state-of-the-art commercial silicon cells. The scalability of processing steps and materials in the manufacture and operation of tandems is considered. The resulting energy payback time and greenhouse gas emission factor of the all-perovskite tandem configuration are 0.35 years and 10.7 g CO₂-eq/kWh, respectively, compared to 1.52 years and 24.6 g CO₂-eq/kWh for the silicon benchmark. Prolonging the lifetime provides a strong technological lever for reducing the carbon footprint such that the perovskite-silicon tandem can outcompete the current benchmark on energy and environmental performance. Perovskite-perovskite tandems with flexible and lightweight form factors further improve the energy and environmental performance by around 6% and thus enhance the potential for large-scale, sustainable deployment.

INTRODUCTION

Industrial development and population growth have led to a surge in global energy consumption over recent decades. To address the increasing scarcity of fossil fuels, there are extensive research efforts focusing on sustainable and renewable energy substitutes. Among the wide array of renewable energy resources, abundant solar energy can be converted into electric power through photovoltaic (PV) technologies without inducing substantial environmental burden. To meet the stringent requirements of efficient deployment of PVs on a global scale, low manufacturing costs and enhanced power conversion efficiency (PCE) are urgently needed.

The emerging metal halide perovskite family has demonstrated great potential as light-harvesting active materials by virtue of excellent light absorption and charge-carrier mobilities (1). Despite record-breaking PCEs (up to 25.2%) (2), single-junction perovskite solar cells stand little chance to outcompete the current benchmark of crystalline silicon (PCE of 27.6%) that dominates the marketplace (2, 3). There are already several commercial (nonperovskite) multi-junction technologies including tandems and triple- and quadruple-junction modules that typically use III to V semiconductors, with promising PCEs that rival and even outperform the benchmark silicon PVs (4). Nevertheless, triple and quadruple junctions are prohibitively expensive for manufacture and terrestrial deployment (5) and thus, to date, are primarily implemented in space applications (6). Therefore, the best chance at large-scale deployment of PVs lies in cost-effective yet high-performance tandems. More encouragingly, perovskites can uniquely enable highly efficient tandems at low cost by integrating the merits of minimal thermalization loss in multi-junction configurations with the beneficial attributes of low-cost processing and high-throughput fabrication (7).

In the shorter term, hybrid perovskite-silicon tandems will pave the way toward widespread deployment of PVs by boosting silicon PVs at little additional cost (8). In the longer term, innovative tandem architectures such as perovskite-perovskite and perovskite-CIGS (copper indium gallium selenide) promise high-performance, inexpensive production of the entire system (4, 7, 9–11), and use in lightweight applications (7). Both of these silicon-free tandem architectures offer great opportunities to achieve moderate PCEs above 30% at reasonable cost and thus are garnering extensive interest in both industry and academia (4, 7, 9–13).

Most of the applied perovskite research is focusing on the enhancement of PCEs and long-term stability for single junctions or tandems (7, 9, 14–19). However, a critical gap in the literature is a critical assessment of the energy use and environmental implications throughout the life cycle of a module, which will be integral to the sustainable development of such innovative technologies (20). Previous life cycle assessment (LCA) studies on perovskite tandems investigated specific tandem stacks, but only considered limited impact categories (8, 21–23) because of the incomplete high-quality life cycle inventory (LCI) datasets in existing databases, and do not consider scalability and industry-compatibility issues. To the best of our knowledge, the existing works do not apply LCA tools to perovskite tandems while maximizing the important potential of scale-up.

Here, we directly assess the environmental impacts of two cutting-edge two-terminal (2T) monolithic perovskite tandem solar cells, namely, perovskite-silicon and perovskite-perovskite configurations (14, 17). First, we estimate their energy payback time (EPBT) and greenhouse gas (GHG) emission factor. In the environmental life cycle impact assessment (LCIA) of tandem PV electricity, the impact categories in the European product environmental footprint recommendation are adopted to unmask their full-spectrum environmental impacts at midpoint level (24). A total of 17 midpoint impact categories are considered with the focus on individual environmental issue. We note that the indicator associated with nuclear waste is not considered because of lack of data. Considering the immaturity of manufacturing techniques and the fluctuation of operating conditions, the energy and environmental performance of tandem solar cells are subject to uncertainty. Thus, a Monte Carlo simulation-based approach is adopted to decipher the uncertainty

¹Systems Engineering, College of Engineering, Cornell University, Ithaca, NY 14853, USA. ²Cavendish Laboratory, University of Cambridge, JJ Thomson Avenue, Cambridge CB3 0HE, UK. ³Department of Chemical Engineering and Biotechnology, University of Cambridge, Philippa Fawcett Drive, Cambridge CB3 0AS, UK. ⁴Robert Frederick Smith School of Chemical and Biomolecular Engineering, Cornell University, Ithaca, NY 14853, USA. ⁵Cornell Atkinson Center for Sustainability, Cornell University, Ithaca, NY 14853, USA.

*Corresponding author. Email: fengqi.you@cornell.edu

of input parameters, followed by a sensitivity analysis quantifying the impacts of parameter deviations. We assume a 15-year lifetime for perovskite-based tandem devices and a 30-year lifetime for the benchmark silicon PVs, following the previous literature on tandem LCA (20). Last, we provide insights into the sustainable development of tandem solar cells that will enhance their future competitiveness with existing commercial technologies. For example, for the perovskite-perovskite tandem, these numbers are further brought down by swapping out encapsulating glass for lightweight substitutes. In addition, periodic module replacement and material recycling strategies will be of great significance for perovskite tandems, especially the perovskite-silicon tandems, to outcompete the current benchmark and accelerate market entry.

Insights for future development

Toward widespread deployment of PV technologies, tandem structures are one of the most promising routes, and perovskites specifically enable inexpensive and high-efficiency tandem fabrication. Because of the larger number and increased complexity of layers in tandem stacks compared to single-junction analogs, tandem will require more intensive inputs in materials and energy. Thus, it is crucial to consider the scalability of the relevant resources and processing steps that industry will continuously innovate to gain more insights with respect to today's laboratory-scale device fabrication. First, precious metal electrodes, including silver and gold, should be substituted with more common metals, such as copper and aluminum (25, 26). Moreover, organic charge-transport materials, such as spiro-OMeTAD {2,2',7,7'-Tetrakis[N,N-di(4-methoxyphenyl)amino]-9,9'-spirobifluorene} and PEDOT:PSS [poly(3,4-ethylenedioxythiophene):poly(styrene sulfonate)], should be replaced with stable inorganic counterparts, typically nickel oxides and tin oxides (27–30). Energy-intensive or unscalable deposition methods, such as high-vacuum thermal evaporation and spin coating, should be replaced with scalable counterparts, such as sputtering and slot-die coating (31, 32). Furthermore, effective and low-cost encapsulation methods should be developed for tandem devices to enhance the stability and thus prolong the lifetime while minimizing the undesirable restraint on module efficiency (31). These may serve as a guide for laboratory-scale tandem stack design toward industry-relevant modules.

Here, we perform holistic LCA studies with an explicit consideration on the scalability issues mentioned above and find that silicon-free tandems are more promising than perovskite-silicon tandems to replace silicon PVs in the short term with respect to environmental factors. As one step toward widespread PV deployment, the perovskite-silicon tandem bears 5.31% more primary energy consumption, yet 5.54% shorter EPBT than the current benchmark. The EPBT is not substantially different from that of silicon PVs, and there is an unexpected proliferation in the GHG emission factor. By eliminating the use of environmentally expensive silicon wafers, the perovskite-perovskite tandem exhibits a 77.8% decrease in primary energy consumption over the perovskite-silicon tandem, while the total energy output is not drastically compromised. This silicon-free tandem architecture shows promisingly small EPBT of 0.35 years compared to 1.44 years for the perovskite-silicon tandem and, in turn, compared to 1.52 years for the current silicon benchmark. For the perovskite-perovskite tandem, the EPBT is reduced to only one-fourth of the silicon PV reference and, more encouragingly, an extremely low GHG emission factor of 10.69 g CO₂-eq/kWh is obtained compared to 46.38 g CO₂-eq/kWh for the perovskite-silicon tandem and, in

turn, compared to merely 24.63 g CO₂-eq/kWh for the benchmark silicon PVs. Through sensitivity analyses, we find that prolonging the lifetime is a critical technological lever for cutting the undesired GHG emission factor down to the level of the current benchmark. By combining the currently high-profile research directions of PCE enhancement and lifetime extension with lightweight applications, periodic module replacement, and hot spot material recycling strategies (33, 34), the carbon mitigation benefits of emerging perovskite tandem technologies will be more pronounced, resulting in a clear commercialization trajectory.

RESULTS

Life cycle inventory

The technical details of the two investigated tandem modules are given in Table 1, and the corresponding schematics including the layer composition and thickness are illustrated in Fig. 1. Note that the LCIs in this LCA study are not directly derived according to the experimental procedures reported in the referenced papers (14, 17) because some materials and processing steps in laboratory-scale fabrication may encounter economic and energy challenges for scale-up. The materials corresponding to energy and environmental hot spots are carefully substituted with suitable counterparts for scalable fabrication and widespread applications, and the PCEs of the reconstructive modules are assumed to be unchanged. For example, silver is replaced with less expensive copper (25, 26), and indium tin oxide is substituted with Al-doped zinc oxide (AZO) (7). There is a large body of literature on this topic, and industry is constantly innovating on those inexpensive yet stable substitutes. As shown in Fig. 1, functional layers marked with an asterisk denote a realistic scalable substitute with respect to the current literature reporting on laboratory cells. The schematics of the prototypical tandem architectures extracted from the referenced papers are also presented in the Supplementary Materials for comparative illustration against Fig. 1. The calibrated LCIs for manufacturing 1-m² modules of perovskite-silicon and perovskite-perovskite tandems, as well as the intact LCI of the current benchmark crystalline silicon, are given in the Supplementary Materials.

Specifically, the LCIs in this study can be categorized into two groups, namely, material inventory and energy inventory. Because the mass and energy balances with respect to multiple key components in the two investigated tandem architectures are not off the shelf in existing literature, comprehensive manufacturing routes are developed and modeled for these chemicals. In this way, the undocumented

Table 1. Technical details of two types of state-of-the-art 2T monolithic tandem solar cells.

	Perovskite-silicon tandem (17)	Perovskite-perovskite tandem (14)
Module efficiency	25.2%	23.1%
Low-bandgap cell	Silicon heterojunction (SHJ) cell	(FA, MA) (Sn, Pb) I ₃ perovskite solar cell
Recombination junction	AZO	AZO
Wide-bandgap cell	(Cs, FA) Pb (I, Br) ₃ perovskite solar cell	(Cs, FA, MA) Pb (I, Br) ₃ perovskite solar cell

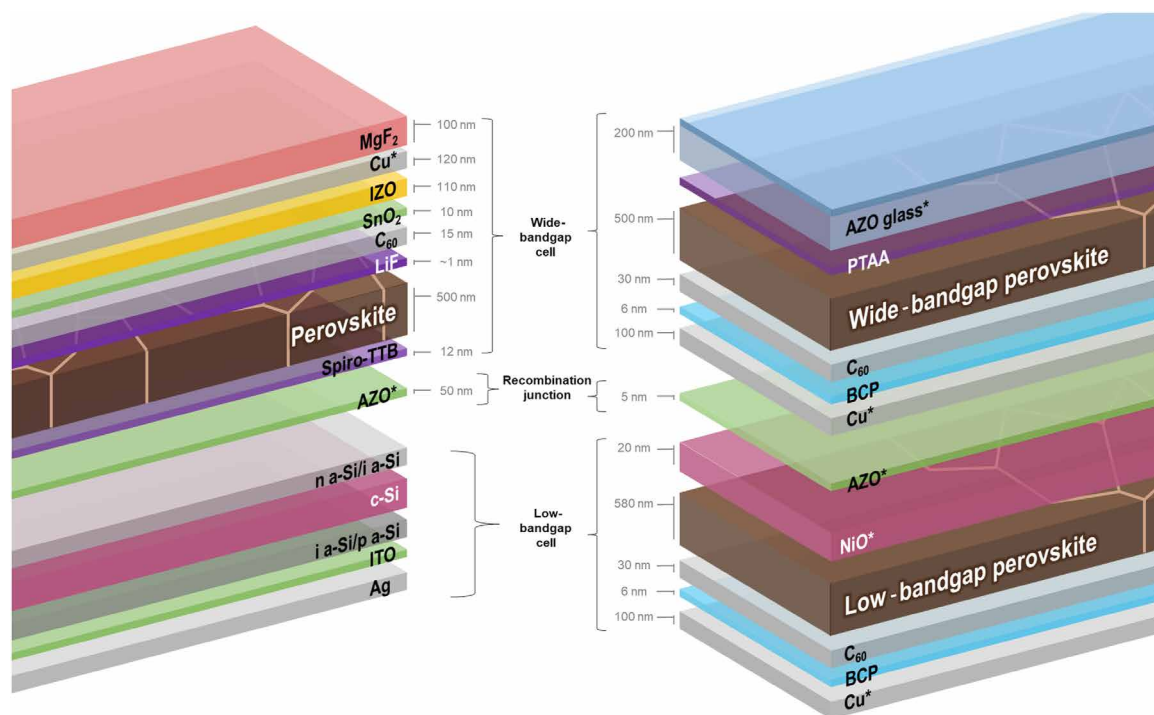


Fig. 1. Schematics of perovskite-silicon tandem solar cell (on the left) and perovskite-perovskite tandem solar cell (on the right). Functional layer with asterisk in the name indicates that the corresponding material has been replaced toward scalable fabrication. No alteration is implemented to the benchmark silicon heterojunction (SHJ) cell.

substances, which are not yet produced at commercial scale, are bridged with those well archived in the existing database; specifically, Ecoinvent (version 3.6; 2019) is used throughout this LCA study (35). Detailed LCIs for these relevant components, such as C_{60} , tin chloride, and cesium bromide, are derived on the basis of the “best available” data in literature and presented in the Supplementary Materials, along with their corresponding impact results. Screen printing, a roll-to-roll compatible process, is adopted to fabricate perovskite layers and other organic charge-transport layers during the deposition of perovskite subcells in both device architectures; the remaining inorganic functional layers are deposited by sputtering (14, 17, 21). Screen printing is a suitable choice because its direct process energy consumption data have been well documented (20, 36), allowing us to make realistic and conservative estimates compared to other more materials-efficient roll-to-roll processing alternatives (31). We note that industry will continue to innovate on both materials and processing steps, and the numbers herein, including the LCIs and the corresponding LCIA results, can thereby serve as conservative upper bounds; other high-efficiency materials and processing routes may be implemented in future work as more data become available. All the processing steps used to assemble the tandem solar cells are driven by electric power, and the power consumption of each processing step is estimated on the basis of equipment power and the corresponding operational time.

Primary energy consumption and carbon footprint

In this section, two prevailing impact indicators in the LCA studies on PV technologies, namely, the primary energy consumption and the carbon footprint (36–43), are estimated and compared between the two investigated tandem architectures as well as with benchmark

silicon PVs. Primary energy consumption accounts for the primary energy embedded in the raw materials and that consumed by processing steps. Carbon footprint measures the global warming potential associated with raw materials and processing steps relative to that of carbon dioxide across the lifetime of a certain production or service system. For both tandem architectures, the low-bandgap subcell serves as the bottom cell, while the wide-bandgap subcell is deemed as the top cell. Functional layers other than those embodied in the bottom cell comprise the “add-on.” For example, the bottom cell in the perovskite-silicon tandem solar cell refers to the silicon heterojunction (SHJ) cell, and the add-on in this configuration embraces the wide-bandgap cell and the recombination junction, as shown in Fig. 1. This “cradle-to-grave” LCA study focuses on land-fill as the end-of-life scenario.

As shown in Fig. 2A, the SHJ bottom cell produces an extremely intensive primary energy consumption of ~ 3500 MJ/m² of module. This is fundamentally due to the substantial inputs in materials and energy during the fabrication of the SHJ cell, especially the energy-intensive purification process of silicon to solar grade, accounting for up to 90% of the total energy required for PV cell production (20, 44, 45). The perovskite-silicon tandem gains in relative PCE by 11.5% (absolute PCE increases from 22.6% for SHJ bottom cell to 25.2% for tandem), exceeding the 5.31% of incremental primary energy consumption induced by the add-on. In contrast, the low-bandgap subcell only accounts for two-thirds of the primary energy consumption and carbon footprint of the wide-bandgap subcell in the perovskite-perovskite configuration. This difference is largely due to the deposition of a much thicker AZO layer during the wide-bandgap subcell fabrication, thus leading to a higher energy consumption. Although the overall PCE of this silicon-free tandem architecture

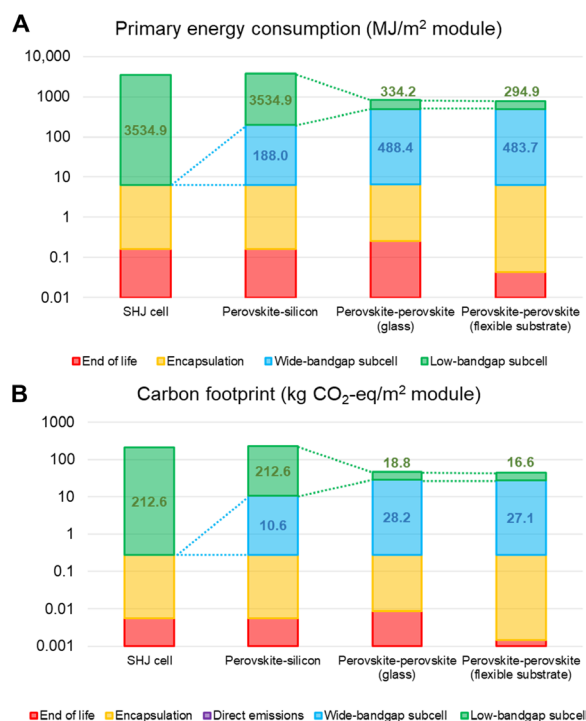


Fig. 2. Overview of primary energy consumption and carbon footprint for the SHJ cell, the perovskite-silicon tandem, and the perovskite-perovskite tandem (on both glass and flexible substrate) on a logarithmic scale. (A) Primary energy consumption breakdowns for the SHJ cell and the two tandem solar cells. **(B)** Carbon footprint breakdowns for the SHJ cell and the two tandem solar cells.

(23.1%) is lower than that of the perovskite-silicon tandem device (25.2%), the total primary energy consumption is only one-fifth of that of the perovskite-silicon tandem device. We note that despite the slightly lower PCE than perovskite-silicon tandems, perovskite-perovskite tandems, as well as perovskite-silicon tandems, will likely attain PCE exceeding 30% with continued improvement in selected materials and processing steps. More encouragingly, perovskite-perovskite tandem architecture demonstrates the capabilities for fabrication on flexible and lightweight substrate as well as large-volume manufacture, e.g., roll-to-roll processing. A resemblance can be observed between the profiles of primary energy consumption and carbon footprint. Notably, the end of life accounts for a lower proportion of the carbon footprint than the primary energy consumption for both perovskite-silicon and perovskite-perovskite tandems. In Fig. 2B, the contribution of the end of life for the flexible perovskite-perovskite tandem becomes even less substantial by virtue of lightweight form factors.

EPBT and GHG emission factor

On the basis of the primary energy consumption and carbon footprint results obtained in the previous section, we calculate the EPBT and GHG emission factor, two important metrics to measure the sustainability of PV technologies. To account for the uncertainty embedded in numerous key input parameters, including the performance ratio, PCE, annual irradiation, primary energy consumption, carbon footprint, and lifetime (46, 47), we adopt a Monte Carlo simulation-based method using the Oracle Crystal Ball (48). The performance ratio is defined as the ratio of actual to theoretically possible energy

output, which evaluates the quality of PV installation and accounts for all potential losses depending on the site, the technology, and the system scale. Notably, lifetime is the overarching influential factor on GHG emission factor, yet there is no reliable lifetime information for perovskite tandem cells in the literature. It is unlikely that widespread rooftop or utility-scale modules would be on the market with a lifetime less than 10 years (maintaining a reasonable performance), and this is also the lifetime value in which module replacement schemes become viable (33). To this end, a conservative lifetime of 15 years is assumed for both tandem devices with stable PCEs during their service life, whereas a 30-year lifetime is assigned to the benchmark silicon PVs, following the assumptions made in a previous tandem LCA study (20).

Figure 3A demonstrates the simulation results for both perovskite-silicon (blue cluster) and perovskite-perovskite (red cluster) tandem solar cells. We obtain an EPBT value of 0.35 ± 0.05 years and GHG emission factor of 10.94 ± 2.20 g CO₂-eq/kWh (mean \pm SD) for perovskite-perovskite tandems. In contrast, the perovskite-silicon tandem device exhibits a longer EPBT (mean value, 1.46; SD, 0.23) by a factor of 4.2 and larger GHG emission factor (mean value, 47.46; SD, 10.08) by a factor of 4.3. Here, we refer back to the benchmark silicon PVs (SHJ cell with a PCE of 22.6%), which has an EPBT of 1.52 years and a GHG emission factor of 24.63 g CO₂-eq/kWh. The large gap between the GHG emission factor of perovskite-silicon tandem and the SHJ cell is attributed to the critical difference in lifetime. This, in turn, puts emphasis on the requirement to prolong the lifetime to reduce the climate impact of emerging tandem technologies. To verify the estimates with respect to EPBT and GHG emission factor, we present a detailed comparison against the results from existing literature on tandem LCA in fig. S3.

Moreover, sensitivity analyses are performed according to the simulation results, as shown in Fig. 4 (A to D). The nominal value for the performance ratio is set to the default value of 0.75 according to Frischknecht *et al.* (24). The electric-to-primary energy conversion coefficient is determined as per the Western Electricity Coordinating Council (WECC) electricity mix according to the Ecoinvent database (49). The same distributions are assigned to the key input parameters according to Gong (36), which are shown in the right-hand-side labels in Fig. 4 (A to D) in terms of mean and (geometric) SD. The minus signs indicate the corresponding input parameters that are in negative correlation with the objective function value and vice versa. The absolute values of percentages inform what fraction each parameter can influence the calculated quantity. The deviation of EPBT from its nominal value is induced by the fluctuations in the performance ratio, the respective primary energy consumption of each subcell, the overall PCE, and the annual insolation. An additional factor, the lifetime, leads to notable variation in the GHG emission factor. The performance ratio can be intuitively identified as the dominant factor among the mutual input parameters that exert influence on both sustainability metrics. The impact of the module efficiency and insolation is much less pronounced. The contributions to these metrics from the low- and wide-bandgap subcells are similar for the perovskite-perovskite tandem, whereas the bottom cell presents substantially higher impacts in the perovskite-silicon tandem architecture due to the large difference in these metrics between the SHJ cell and perovskite solar cell. Other factors, such as device degradation (beyond imposing a limited lifetime of 15 years), that may affect the energy yield are not considered in this work but should be carefully addressed in future work.

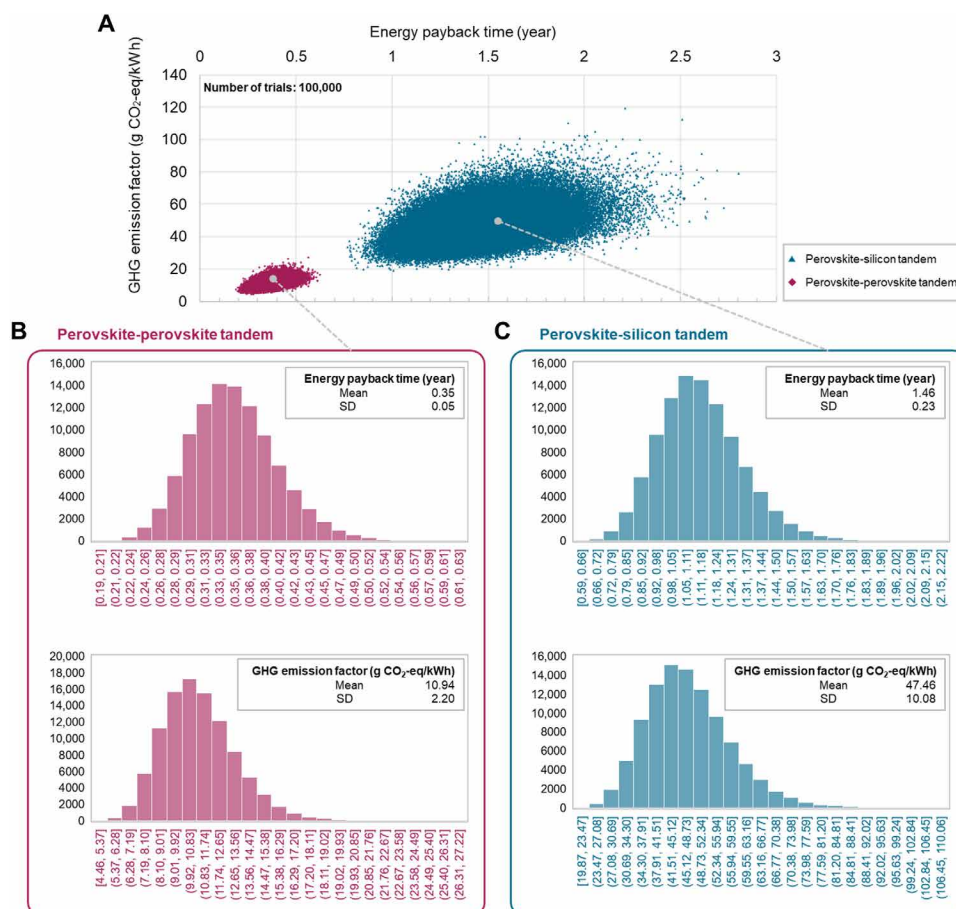


Fig. 3. Uncertainty analysis results for the two tandem technologies. (A) Monte Carlo simulation results for perovskite-perovskite tandem (red cluster) and perovskite-silicon tandem (blue cluster). (B) Probability distribution for the EPBT and the GHG emission factor of the perovskite-perovskite tandem solar cell. (C) Probability distribution for the EPBT and the GHG emission factor of the perovskite-silicon tandem solar cell.

Furthermore, we note that lifetime is the dominant influential factor on GHG emission factor for both tandem modules. To gain more insights into how GHG emission factor comes down with respect to the key investigated parameters, namely, the PCE and lifetime, the corresponding impacts are quantified and illustrated in Fig. 4 (E and F) for the perovskite-silicon tandem and perovskite-perovskite tandem, respectively. Each colored area corresponds to a successive range of GHG emission factor, as denoted in the legend, and the frontiers between adjacent colored areas represent the isolines of the GHG emission factor. The closer the curve is to the upper right corner, the lower the GHG emission factor. The dotted curve corresponds to the GHG emission factor of the current benchmark. The PCE is upper-bounded by the Shockley-Queisser limit (20). As illustrated in Fig. 4E, the extreme points of the dotted curve correspond to [16 to 17 years, 42.0%] and [30 years, 23.7%] ([lifetime, PCE]). We find that the perovskite-silicon tandem cannot achieve the GHG emission factor as low as the benchmark by merely enhancing the PCE but can make it by prolonging the 15-year lifetime to 28 to 29 years while retaining the current PCE, which is hard to realize in the short run. On the contrary, Fig. 4F shows that the perovskite-perovskite tandem can outcompete the benchmark silicon PVs on these metrics with the given PCE and lifetime, which is readily feasible. Further improving the PCE or extending the lifetime will en-

able such a tandem configuration with even lower GHG emissions and thus the potential for widespread deployment within a relatively shorter term compared to the perovskite-silicon tandems. Simultaneous enhancement of PCE and long-term stability will bring down the GHG emission factor more efficiently through synergistic effects.

The results show that perovskite-perovskite tandems stand more chance of outcompeting the current benchmark, while the perovskite-silicon configuration may encounter more impediments to commercialization based on these environmental metrics. We emphasize here that it is insufficient to merely focus on PCE and lifetime for the pursuit of widespread deployment, especially for the perovskite-silicon tandem. Recycling the environmental hot spots from decommissioned modules (34), or replacing modules periodically with more advanced systems, likely enables more environmentally sustainable tandem solar cells (33). On the one hand, effective recycling alleviates energy use and environmental burden via the tenet of an avoided burden approach, namely, borrowing the environmental loans from future generations for synthetic capital that is likely to be recycled in the future (50). On the other hand, a module replacement process has less requirement for long-lived modules and therefore further empowers the near-term market entry of emerging perovskite tandems (33). Further studies are needed to systematically assess the

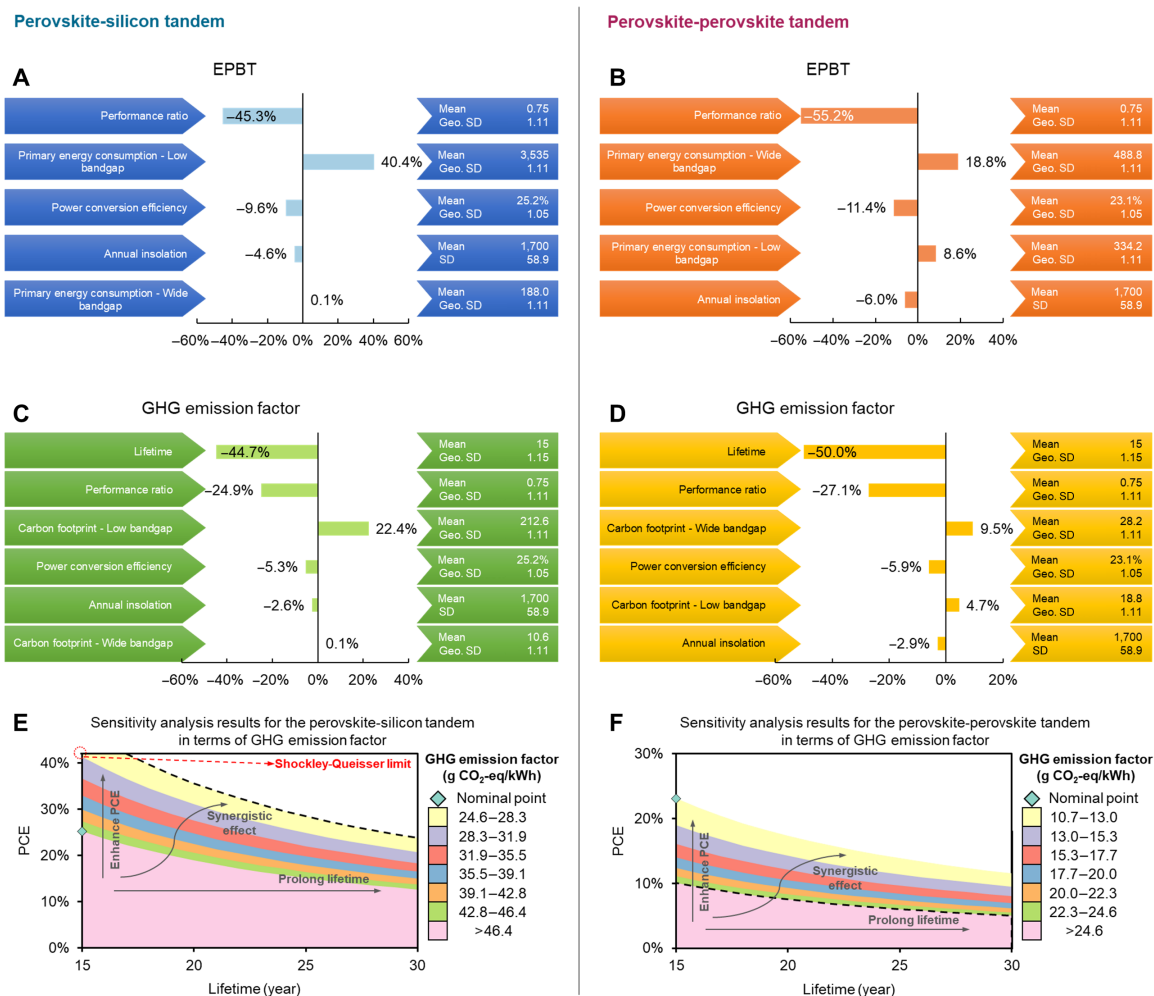


Fig. 4. Sensitivity analysis results. (A) Sensitivity analysis results for the perovskite-silicon tandem solar cell in terms of EPBT. (B) Sensitivity analysis results for the perovskite-perovskite tandem solar cell in terms of EPBT. (C) Sensitivity analysis results for the perovskite-silicon tandem solar cell in terms of GHG emission factor. (D) Sensitivity analysis results for the perovskite-perovskite tandem solar cell in terms of GHG emission factor. (E) Effects of lifetime and PCE on the GHG emission factor of perovskite-silicon tandem solar cell. (F) Effects of lifetime and PCE on the GHG emission factor of perovskite-perovskite tandem solar cell. In the last two charts, the diamond icons stand for the base-case points corresponding to the current lifetime and PCE of each tandem configuration. The frontiers between adjacent colored areas represent the isolines of GHG emission factor. The dotted curve corresponds to the GHG emission factor of the current benchmark. The PCE is upper-bounded by the Shockley-Queisser limit.

benefit of periodic module replacement during the use stage of tandems, which is beyond the scope of this work. The current study focuses on the life cycle environmental impacts during the raw material acquisition, energy supply, and manufacturing of panels, with construction process and replacement stages excluded, following previous LCA studies (20, 36, 51).

Full spectrum of life cycle environmental impacts

Figure 5 shows the full-spectrum environmental profiles of 1 m² of the perovskite-silicon tandem solar cell according to the specified LCIA approach following the same selection by Frischknecht *et al.* (24). To intuitively demonstrate the results, the overall life cycle environmental impacts are divided into four groups, namely, environmental impacts associated with raw materials in the wide-bandgap subcell, processing steps during wide-bandgap subcell fabrication, raw materials in the low-bandgap subcell, and processing steps during

low-bandgap subcell fabrication. The color corresponding to each metric is consistent with the color of the raw material or processing step that contributes most to that metric. As shown in Fig. 5A, copper is one of the environmentally expensive factors that dominate several impact indicators at the midpoint level, including particulate matter/respiratory effects, acidification, and freshwater eutrophication. This is primarily because metal production always requires intensive inputs in materials and energy, as well as the subsequent environmental deterioration along with the mining activities. We note that copper is still much less impactful than silver and gold typically used in laboratory-scale cells, and it is unlikely that a metal can be avoided for large-scale modules. When it comes to the assembling of the perovskite top cell, MgF₂ sputtering dominates all investigated environmental metrics. Similar results can be observed in Fig. 5 (C and D) for environmental hot spot identification in the SHJ bottom cell. The crystalline silicon wafer accounts for the highest proportions

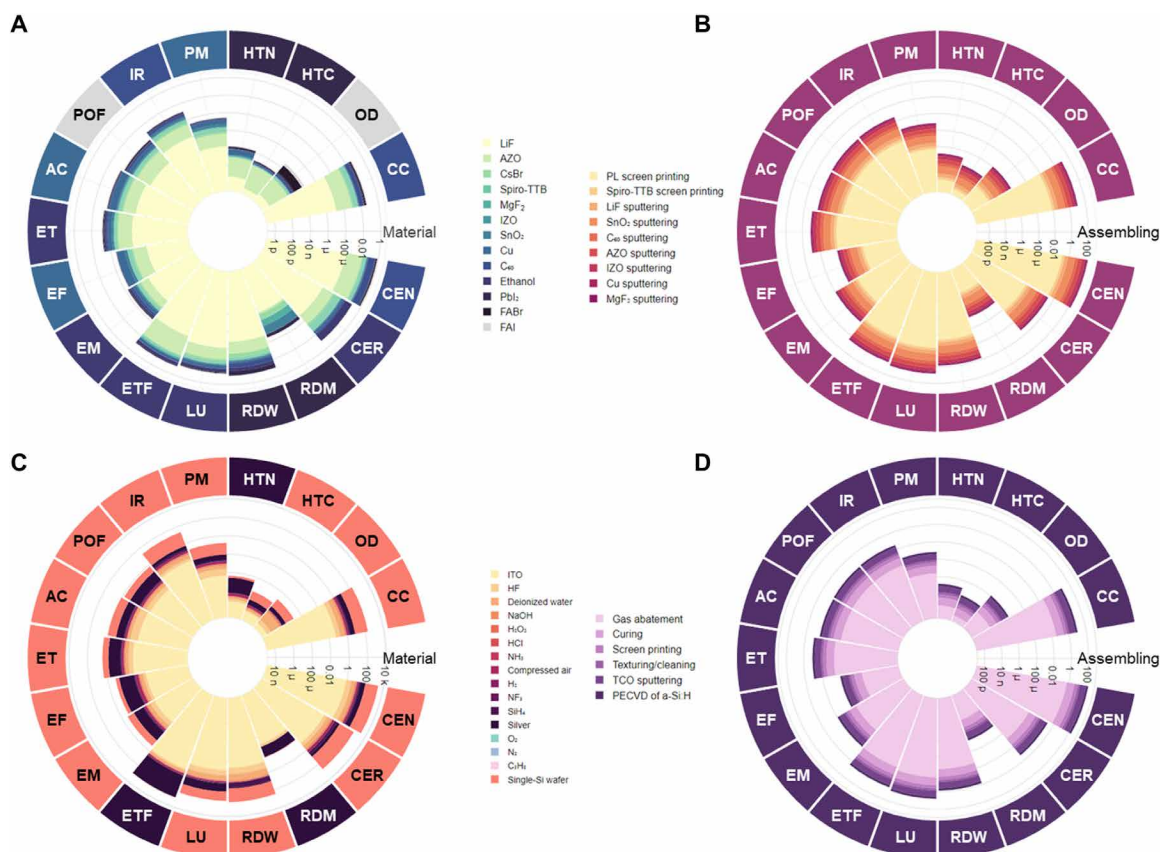


Fig. 5. Full-spectrum life cycle environmental impacts of 1 m² of the perovskite-silicon tandem solar cell on a logarithmic scale. Acronyms go counter clockwise: climate change (CC) (kg CO₂ eq); ozone depletion (OD) (kg CFC-11 eq); human toxicity, cancer effects (HTC) (CTUh, c); human toxicity, non-cancer effects (HTN) (CTUh, n-c); particulate matter/respiratory effects (PM) (kg PM_{2.5} eq); ionizing radiation, human health (IR) (kg U235 eq); photochemical ozone formation (POF) (kg NMVOC eq); acidification (AC) (mol H⁺ eq); eutrophication, terrestrial (ET) (mol N eq); eutrophication, fresh water (EF) (kg P eq); eutrophication, marine (EM) (kg N eq); ecotoxicity, fresh water (ETF) (CTUe); land use (LU) (kg C deficit); resource depletion, water (RDW) (m³ water eq); resource depletion, mineral, fossil, renewable (RDM) (kg Sb eq); cumulative energy demand, renewable (CER) (MJ eq); cumulative energy demand, non-renewable (CEN) (MJ eq). (A) Life cycle environmental impacts embedded in the raw materials of the add-on. (B) Life cycle environmental impacts associated with the assembling phase of the add-on. (C) Life cycle environmental impacts embedded in the raw materials of the SHJ bottom cell (for both perovskite-silicon tandem and benchmark silicon PVs). (D) Life cycle environmental impacts associated with assembling phase of the SHJ bottom cell (for both perovskite-silicon tandem and benchmark silicon PVs).

for most of the impact categories, and the plasma-enhanced chemical vapor deposition dominates the assembling phase. The full-spectrum life cycle environmental impact results for the perovskite-perovskite tandem module are given in the Supplementary Materials. For the add-on fabrication in the perovskite-perovskite architecture, the use of solar glass dominates the material-embedded environmental impacts for most of the impact categories, while AZO sputtering is the major contributor for the assembling phase. The profiles for the bottom cell look more dynamic: SnI₂ and methylammonium iodide (MAI) are identified as the environmental hot spots, and copper sputtering predominates the assembling phase.

Enabling flexible perovskite-perovskite tandems

As mentioned in previous sections, perovskite-perovskite tandems pave the way toward not only very low production cost but also the potential for flexible and lightweight applications, which will, in turn, bring down other costs including installation. To quantify how far the investigated sustainability metrics, namely, EPBT and GHG emission factor, can come down, additional analysis is performed by swapping out the glass substrate for a flexible polyethylene terephthalate

(PET)-based counterpart. In addition to the substrate material, high-temperature processing steps should be replaced, e.g., the sputtering of nickel oxide, which is usually annealed at 300° to 500°C for sufficiently enhanced crystallinity and conductivity (31). This high temperature range, however, is generally not compatible with deposition on flexible substrates. Hence, when fabricating tandem modules on flexible substrates, it is imperative to adopt alternative deposition steps with milder processing conditions (e.g., screen printing) for depositing layers such as nickel oxide, which is becoming the norm for laboratory-based research (31). The perovskite-perovskite tandem on flexible PET-based substrate leads to an EPBT of 0.33 years (0.02 years shorter than that of the glass-based tandem) and GHG emission factor of 9.96 g CO₂-eq/kWh (0.73 g CO₂-eq/kWh lower than that of the glass-based tandem). The detailed environmental profiles for the perovskite-perovskite tandem based on glass and flexible substrate are systematically compared using the selected LCIA method, as shown in Fig. 6. For flexible and lightweight applications, environmentally expensive solar glass is substituted with cheaper plastic, and high-temperature operations are excluded from the feasible processing space, thus leading to reduced energy consumption

and environmental impacts. As for the absolute value of each midpoint indicator, ionizing radiation (human health) (0.25 kg U235 eq. → 0.21 kg U235 eq., 14.32%), land use (32.07 kg C deficit → 27.38 kg C deficit, 14.62%), and cumulative energy demand (renewable) (2.99 MJ eq. → 2.51 MJ eq., 16.19%) demonstrate the most drastic decrease ([value for glass-based tandem → value for lightweight substrate-based tandem, percentage decrease]), while the remaining impact categories show lower percentage reductions, up to 12.40%, through the use of lightweight substrates. Future research should be directed to the development of flexible perovskite-perovskite tandem modules.

DISCUSSION

In this work, an extensive cradle-to-grave LCA was performed for two state-of-the-art tandem architectures, namely, the perovskite-silicon and perovskite-perovskite tandems, which also takes into consideration the uncertainties of key input parameters. By combining perovskites with crystalline silicon PVs, the perovskite-silicon tandems presented 5.54% net gain in EPBT over the current silicon single-junction benchmark. By diminishing the use of crystalline silicon wafers, perovskite-perovskite tandems provided an even more promising avenue that could accelerate the development of PVs toward the cheapest and most ubiquitously used power source. The resulting EPBT and GHG emission factor of such a tandem configuration are as low as 0.35 years and 10.69 g CO₂-eq/kWh, respectively, and these numbers further come down to 0.33 years and 9.96 g CO₂-eq/kWh when adopting lightweight form factors. Through sensitivity analysis, substituting environmental hot spot materials and processing steps, prolonging lifetime, and improving performance

ratio were identified as feasible approaches to enhance the sustainability of tandem modules, among which prolonging lifetime was found to be the strongest technological lever for carbon mitigation. For perovskite tandem solar cells, especially the perovskite-silicon structure, periodic module replacement and material recycling strategies should also be implemented to outcompete the benchmark silicon PV technologies and accelerate market entry. Moreover, adopting materials and processing steps that are even more compatible with scalable fabrication is also a critical facet in the sustainable development of tandem solar cells.

MATERIALS AND METHODS

Four-phase LCA approach

Goal and scope definition

We performed a holistic LCA to estimate and compare the energy use and environmental implications throughout the life cycle of two types of state-of-the-art tandem architectures, including one perovskite-perovskite tandem solar cell and one perovskite-silicon tandem solar cell (14, 17). The results are, in turn, compared with the current benchmark of crystalline silicon. The system boundary of the cradle-to-grave life cycle of tandem solar cells embraces four stages from raw material acquisition through module assembling, module use, and end-of-life disposal. Because module area is an important metric used to quantify the scale of single- and multi-junctions (20, 36), the functional unit of this LCA is defined as 1 m² of envisioned tandem device. We assume that all the manufacturing of raw materials, assembling of tandem solar modules, and installation take place on the west coast of the United States. The electric-to-primary energy

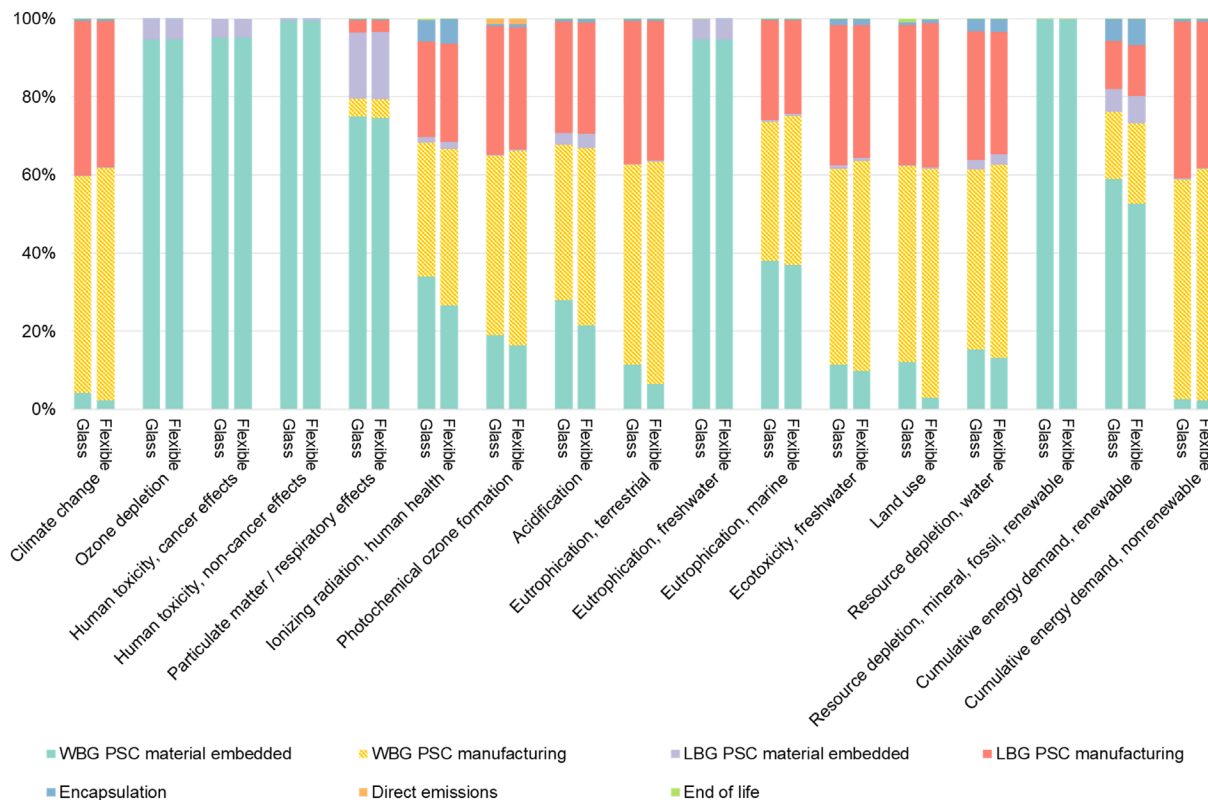


Fig. 6. Comparative environmental profiles for perovskite-perovskite tandem based on glass and flexible substrates. WBG and LBG refer to wide-bandgap and low-bandgap, respectively; PSC stands for perovskite solar cell.

conversion coefficient ϵ is determined on the basis of the WECC electricity mix according to the Ecoinvent database (49).

LCI analysis

The LCIs are the comprehensive inventories of material and energy flow across all life cycle stages of the tandem devices. The LCIs in this LCA account for both the LCIs of raw material synthesis and those of device fabrication. LCI analyses are not required for most of raw materials whose LCI data are either well archived in the off-the-shelf database or extractable from the existing literature but are imperative for the other components. The LCIs for the latter group of substances are derived according to the manufacturing routes that are established on the basis of the respective synthesis mechanism, physical and chemical properties of all relevant substances, and energy consumption of processing steps. The LCIs of device fabrication are estimated in accordance with the best available laboratory-scale fabrication procedures. All the LCIs are converted to align with the pre-defined functional unit.

Life cycle impact assessment

In the LCIA phase, the LCI results are translated on the basis of selected LCIA approaches into the corresponding indicators. In this LCA, we focus on the cumulative energy demand (or primary energy consumption) (35), the Intergovernmental Panel on Climate Change (IPCC) 2013 (climate change) method (52), and other midpoint impact categories (24). Because PVs are considered as alternative energy suppliers that are capable of generating greener power, it is of great significance to comprehend the energy profile and carbon footprint with respect to the tandem solar cells. A total of 17 midpoint indicators are used following the recommendation by Frischknecht *et al.* (24), including climate change (CC); ozone depletion (OD); human toxicity, cancer effects (HTC); human toxicity, non-cancer effects (HTN); particulate matter/respiratory effects (PM); ionizing radiation, human health (IR); photochemical ozone formation (POF); acidification (AC); eutrophication, terrestrial (ET); eutrophication, fresh water (EF); eutrophication, marine (EM); ecotoxicity, fresh water (ETF); land use (LU); resource depletion, water (RDW); resource depletion, mineral, fossil, renewable (RDM); cumulative energy demand, renewable (CER); and cumulative energy demand, non-renewable (CEN).

Interpretation

The LCIA results of the two tandem solar cells convey important information about the contributions of materials and processing steps to different impact indicators. The major impact contributors can be intuitively identified as environmental hot spots via simple observation. Through Monte Carlo simulation (48), uncertainty and sensitivity analyses are conducted to reveal the resulting distributions of prevalent sustainability metrics, namely, EPBT and GHG emission factor, and identify the most influential factor. On the basis of these results, more insightful suggestions are made toward the sustainable development of tandem solar cells.

EPBT and GHG emission factor

EPBT measures the time needed to compensate for the energy consumption during the manufacture of the solar cells (22, 53, 54). EPBT can be determined on the basis of the primary energy consumption, and the explicit formulation is shown in Eq. 1

$$EPBT = \frac{PEC}{\epsilon \cdot IS \cdot \eta \cdot PR} \quad (1)$$

where PEC is the primary energy consumption (MJ per m^2 of module) associated with the investigated PV modules, ϵ refers to the electric-to-primary energy conversion coefficient (MJ per kWh), IS denotes the annual insolation (kWh per m^2 per year), η stands for the PCE (%), and PR represents the performance ratio (%).

GHG emission factor (FC^{GHG}) indicates the GHG emissions per kWh of electric power generated by the investigated solar cell across its lifetime. The GHG emission factor is derived on the basis of carbon footprint as follows

$$FC^{GHG} = \frac{FP^{carbon}}{IS \cdot \eta \cdot PR \cdot LT} \quad (2)$$

where FP^{carbon} refers to the life cycle carbon footprint (g CO_2 -eq per m^2 of module) of PV modules and LT represents the lifetime (years).

SUPPLEMENTARY MATERIALS

Supplementary material for this article is available at <http://advances.sciencemag.org/cgi/content/full/6/31/eabb0055/DC1>

REFERENCES AND NOTES

1. NREL, *Photovoltaic Research: Perovskite Solar Cells* (NREL, 2019); <https://nrel.gov/pv/perovskite-solar-cells.html>.
2. NREL, *NREL Transforming Energy: Best Research-Cell Efficiency Chart* (NREL, 2019); <https://nrel.gov/pv/cell-efficiency.html>.
3. C. Philibert, *Technology Roadmap: Solar Photovoltaic Energy* (International Energy Agency, 2014).
4. D. P. McMeekin, S. Mahesh, N. K. Noel, M. T. Klug, J. Lim, J. H. Warby, J. M. Ball, L. M. Herz, M. B. Johnston, H. J. Snaith, Solution-processed all-perovskite multi-junction solar cells. *Joule* **3**, 387–401 (2019).
5. M. T. Höranter, T. Leijtens, M. E. Ziffer, G. E. Eperon, M. G. Christoforo, M. D. McGehee, H. J. Snaith, The potential of multijunction perovskite solar cells. *ACS Energy Lett.* **2**, 2506–2513 (2017).
6. F. Lang, M. Jošt, K. Frohna, A. A. Ashouri, A. R. Bowman, T. Bertram, A. B. Morales-Vilches, E. M. Tennyson, K. Galkowski, B. Stannowski, C. A. Kaufmann, R. Schlattmann, J. Bundesmann, A. Denker, J. Rappich, S. Albrecht, H.-C. Neitzert, N. H. Nickel, S. D. Stranks, Radiation hardness of perovskite/silicon and perovskite/CIGS tandem solar cells under proton irradiation, in *Proceedings of nanoGe Fall Meeting 19 (NFM19)*, Berlin, Germany, 3 to 8 November 2019.
7. A. F. Palmstrom, G. E. Eperon, T. Leijtens, R. Prasanna, S. N. Habisreutinger, W. Nemeth, E. A. Gaubling, S. P. Dunfield, M. Reese, S. Nanayakkara, T. Moot, J. Werner, J. Liu, B. To, S. T. Christensen, M. D. McGehee, M. F. A. M. van Hest, J. M. Luther, J. J. Berry, D. T. Moore, Enabling flexible all-perovskite tandem solar cells. *Joule* **3**, 2193–2204 (2019).
8. M. Monteiro Lunardi, A. W. Y. Ho-Baillie, J. P. Alvarez-Gaitan, S. Moore, R. Corkish, A life cycle assessment of perovskite/silicon tandem solar cells. *Prog. Photovolt.* **25**, 679–695 (2017).
9. D. Zhao, C. Chen, C. Wang, M. M. Junda, Z. Song, C. R. Grice, Y. Yu, C. Li, B. Subedi, N. J. Podraza, X. Zhao, G. Fang, R.-G. Xiong, K. Zhu, Y. Yan, Efficient two-terminal all-perovskite tandem solar cells enabled by high-quality low-bandgap absorber layers. *Nat. Energy* **3**, 1093–1100 (2018).
10. H. Shen, T. Duong, J. Peng, D. Jacobs, N. Wu, J. Gong, Y. Wu, S. K. Karuturi, X. Fu, K. Weber, X. Xiao, T. P. White, K. Catchpole, Mechanically-stacked perovskite/CIGS tandem solar cells with efficiency of 23.9% and reduced oxygen sensitivity. *Energy Environ. Sci.* **11**, 394–406 (2018).
11. M. Langenhorst, B. Sautter, R. Schmager, J. Lehr, E. Ahlswede, M. Powalla, U. Lemmer, B. S. Richards, U. W. Paetzold, Energy yield of all thin-film perovskite/CIGS tandem solar modules. *Prog. Photovolt.* **27**, 290–298 (2019).
12. Z. Li, Y. Zhao, X. Wang, Y. Sun, Z. Zhao, Y. Li, H. Zhou, Q. Chen, Cost analysis of perovskite tandem photovoltaics. *Joule* **2**, 1559–1572 (2018).
13. S. Albrecht, B. Rech, Perovskite solar cells: On top of commercial photovoltaics. *Nat. Energy* **2**, 16196 (2017).
14. J. Tong, Z. Song, D. H. Kim, X. Chen, C. Chen, A. F. Palmstrom, P. F. Ndione, M. O. Reese, S. P. Dunfield, O. G. Reid, J. Liu, F. Zhang, S. P. Harvey, Z. Li, S. T. Christensen, G. Teeter, D. Zhao, M. M. Al-Jassim, M. F. A. M. van Hest, M. C. Beard, S. E. Shaheen, J. J. Berry, Y. Yan, K. Zhu, Carrier lifetimes of >1 μ s in Sn-Pb perovskites enable efficient all-perovskite tandem solar cells. *Science* **364**, 475–479 (2019).

15. G. E. Eperon, T. Leijtens, K. A. Bush, R. Prasanna, T. Green, J. T. W. Wang, D. P. McMeekin, G. Volonakis, R. L. Milot, R. May, A. Palmstrom, D. J. Slotcavage, R. A. Belisle, J. B. Patel, E. S. Parrott, R. J. Sutton, W. Ma, F. Moghadam, B. Conings, A. Babayigit, H.-G. Boyen, S. Bent, F. Giustino, L. M. Herz, M. B. Johnston, M. D. McGehee, H. J. Snaith, Perovskite-perovskite tandem photovoltaics with optimized band gaps. *Science* **354**, 861–865 (2016).
16. G. E. Eperon, M. T. Hörantner, H. J. Snaith, Metal halide perovskite tandem and multiple-junction photovoltaics. *Nat. Rev. Chem.* **1**, 0095 (2017).
17. F. Sahlji, J. Werner, B. A. Kamino, M. Bräuninger, R. Monnard, B. Paviet-Salomon, L. Barraud, L. Ding, J. J. Diaz Leon, D. Sacchetto, G. Cattaneo, M. Despeisse, M. Boccard, S. Nicolay, Q. Jeangros, B. Niesen, C. Ballif, Fully textured monolithic perovskite/silicon tandem solar cells with 25.2% power conversion efficiency. *Nat. Mater.* **17**, 820–826 (2018).
18. J. Werner, C.-H. Weng, A. Walter, L. Fesquet, J. P. Seif, S. De Wolf, B. Niesen, C. Balli, Efficient monolithic perovskite/silicon tandem solar cell with cell area >1 cm². *J. Phys. Chem. Lett.* **7**, 161–166 (2016).
19. J. Werner, B. Niesen, C. Ballif, Perovskite/silicon tandem solar cells: Marriage of convenience or true love story?—An overview. *Adv. Mater. Interfaces* **5**, 1700731 (2018).
20. I. Celik, A. B. Phillips, Z. Song, Y. Yan, R. J. Ellingson, M. J. Heben, D. Apul, Environmental analysis of perovskites and other relevant solar cell technologies in a tandem configuration. *Energ. Environ. Sci.* **10**, 1874–1884 (2017).
21. A. Louwen, W. G. J. van Sark, R. E. I. Schropp, W. C. Turkenburg, A. P. C. Faaij, Life-cycle greenhouse gas emissions and energy payback time of current and prospective silicon heterojunction solar cell designs. *Prog. Photovolt.* **23**, 1406–1428 (2015).
22. I. Celik, A. B. Phillips, Z. Song, Y. Yan, R. J. Ellingson, M. J. Heben, D. Apul, Energy payback time (EPBT) and energy return on energy invested (EROI) of perovskite tandem photovoltaic solar cells. *IEEE J. Photovolt.* **8**, 305–309 (2018).
23. R. Itten, M. Stucki, Highly efficient 3rd generation multi-junction solar cells using silicon heterojunction and perovskite tandem: Prospective life cycle environmental impacts. *Energies* **10**, 841 (2017).
24. R. Frischknecht, G. Heath, M. Rauegi, P. Sinha, M. de Wild-Scholten, *Methodology Guidelines on Life Cycle Assessment of Photovoltaic Electricity* (National Renewable Energy Laboratory, 2016).
25. L. Wang, G.-R. Li, Q. Zhao, X.-P. Gao, Non-precious transition metals as counter electrode of perovskite solar cells. *Energy Storage Mater.* **7**, 40–47 (2017).
26. J. Trube, *International Technology Roadmap for Photovoltaic (ITRPV)* (VDMA Photovoltaic Equipment, 2018).
27. Z. Liu, J. Chang, Z. Lin, L. Zhou, Z. Yang, D. Chen, C. Zhang, S. F. Liu, Y. Hao, High-performance planar perovskite solar cells using low temperature, solution-combustion-based nickel oxide hole transporting layer with efficiency exceeding 20%. *Adv. Energy Mater.* **8**, 1703432 (2018).
28. Q. Jiang, Z. Chu, P. Wang, X. Yang, H. Liu, Y. Wang, Z. Yin, J. Wu, X. Zhang, J. You, Planar-structure perovskite solar cells with efficiency beyond 21%. *Adv. Mater.* **29**, 1703852 (2017).
29. K. X. Steirer, J. P. Chesin, N. E. Widjonarko, J. J. Berry, A. Miedaner, D. S. Ginley, D. C. Olson, Solution deposited NiO thin-films as hole transport layers in organic photovoltaics. *Organic Electron.* **11**, 1414–1418 (2010).
30. J. You, C.-C. Chen, L. Dou, S. Murase, H.-S. Duan, S. A. Hawks, T. Xu, H. J. Son, L. Yu, G. Li, Y. Yang, Metal oxide nanoparticles as an electron-transport layer in high-performance and stable inverted polymer solar cells. *Adv. Mater.* **24**, 5267–5272 (2012).
31. Z. Li, T. R. Klein, D. H. Kim, M. Yang, J. J. Berry, M. F. A. M. van Hest, K. Zhu, Scalable fabrication of perovskite solar cells. *Nat. Rev. Mater.* **3**, 18017 (2018).
32. J. B. Whitaker, D. H. Kim, B. W. Larson, F. Zhang, J. J. Berry, M. F. A. M. van Hest, K. Zhu, Scalable slot-die coating of high performance perovskite solar cells. *Sustainable Energy Fuels* **2**, 2442–2449 (2018).
33. J. Jean, M. Woodhouse, V. Bulović, Accelerating photovoltaic market entry with module replacement. *Joule* **3**, 2824–2841 (2019).
34. B. J. Kim, D. H. Kim, S. L. Kwon, S. Y. Park, Z. Li, K. Zhu, H. S. Jung, Selective dissolution of halide perovskites as a step towards recycling solar cells. *Nat. Commun.* **7**, 11735 (2016).
35. Ecoinvent version 3.6 (Ecoinvent Centre, 2019); <https://ecoinvent.org/>.
36. J. Gong, S. B. Darling, F. You, Perovskite photovoltaics: Life-cycle assessment of energy and environmental impacts. *Energ. Environ. Sci.* **8**, 1953–1968 (2015).
37. N. Espinosa, R. Garcia-Valverde, F. C. Krebs, Life-cycle analysis of product integrated polymer solar cells. *Energ. Environ. Sci.* **4**, 1547–1557 (2011).
38. M. M. de Wild-Scholten, Energy payback time and carbon footprint of commercial photovoltaic systems. *Solar Energy Mater. Solar Cells* **119**, 296–305 (2013).
39. N. Espinosa, M. Hösel, D. Angmo, F. C. Krebs, Solar cells with one-day energy payback for the factories of the future. *Energ. Environ. Sci.* **5**, 5117–5132 (2012).
40. E. A. Alsema, E. Nieuwlaar, Energy viability of photovoltaic systems. *Energy Policy* **28**, 999–1010 (2000).
41. V. M. Fthenakis, H. C. Kim, E. Alsema, Emissions from photovoltaic life cycles. *Environ. Sci. Technol.* **42**, 2168–2174 (2008).
42. M. A. Huijbregts, L. J. A. Rombouts, S. Hellweg, R. Frischknecht, A. J. Hendriks, D. Van de Meent, A. M. J. Ragas, L. Reijnders, J. Struijs, Is cumulative fossil energy demand a useful indicator for the environmental performance of products? *Environ. Sci. Technol.* **40**, 641–648 (2006).
43. N. Stylos, C. Koroneos, Carbon footprint of polycrystalline photovoltaic systems. *J. Clean. Prod.* **64**, 639–645 (2014).
44. N. Jungbluth, Life cycle assessment of crystalline photovoltaics in the Swiss ecoinvent database. *Prog. Photovolt.* **13**, 429–446 (2005).
45. V. M. Fthenakis, H. C. Kim, Photovoltaics: Life-cycle analyses. *Solar Energy* **85**, 1609–1628 (2011).
46. D. Yue, P. Khatav, F. You, S. B. Darling, Deciphering the uncertainties in life cycle energy and environmental analysis of organic photovoltaics. *Energ. Environ. Sci.* **5**, 9163–9172 (2012).
47. S. B. Darling, F. You, T. Veselka, A. Velosa, Assumptions and the levelized cost of energy for photovoltaics. *Energ. Environ. Sci.* **4**, 3133–3139 (2011).
48. D. Welsman, Using Monte Carlo simulation with Oracle® Crystal Ball to teach business students sampling distribution concepts. *Bus. Educ. Innov. J.* **7**, 59–63 (2015).
49. K. Treyer, C. Bauer, Life cycle inventories of electricity generation and power supply in version 3 of the ecoinvent database—Part I: Electricity generation. *Int. J. Life Cycle Assess.* **21**, 1236–1254 (2016).
50. R. Frischknecht, LCI modelling approaches applied on recycling of materials in view of environmental sustainability, risk perception and eco-efficiency. *Int. J. Life Cycle Assess.* **15**, 666–671 (2010).
51. N. Espinosa, L. Serrano-Luján, A. Urbina, F. C. Krebs, Solution and vapour deposited lead perovskite solar cells: Ecotoxicity from a life cycle assessment perspective. *Solar Energy Mater. Solar Cells* **137**, 303–310 (2015).
52. T. Stocker, D. Qin, G.-K. Plattner, M. Tignor, S.K. Allen, J. Boschung, A. Nauels, Y. Xia, V. Bex, P.M. Midgley, IPCC, 2013: *Climate Change 2013: The Physical Science Basis. Contribution of Working Group I to the Fifth Assessment Report of the Intergovernmental Panel on Climate Change* (Intergovernmental Panel on Climate Change, 2013).
53. K. P. Bhandari, J. M. Collier, R. J. Ellingson, D. S. Apul, Energy payback time (EPBT) and energy return on energy invested (EROI) of solar photovoltaic systems: A systematic review and meta-analysis. *Renew. Sustain. Energy Rev.* **47**, 133–141 (2015).
54. M. Rauegi, S. Bargigli, S. Ulgiati, Life cycle assessment and energy pay-back time of advanced photovoltaic modules: CdTe and CIS compared to poly-Si. *Energy* **32**, 1310–1318 (2007).
55. A. Anctil, C. W. Babbitt, R. P. Raffaele, B. J. Landi, Material and energy intensity of fullerene production. *Environ. Sci. Technol.* **45**, 2353–2359 (2011).
56. J. Zhang, X. Gao, Y. Deng, Y. Zha, C. Yuan, Comparison of life cycle environmental impacts of different perovskite solar cell systems. *Solar Energy Mater. Solar Cells* **166**, 9–17 (2017).
57. J.-A. Alberola-Borrás, R. Vidal, I. Mora-Seró, Evaluation of multiple cation/anion perovskite solar cells through life cycle assessment. *Sustainable Energy Fuels* **2**, 1600–1609 (2018).

Acknowledgments

Funding: This work is supported, in part, by the National Science Foundation (NSF) CAREER Award (CBET-1643244) and the Cornell Atkinson Center for Sustainability. S.D.S. acknowledges support from the Royal Society and Tata Group (UF150033). **Author contributions:** F.Y. conceived the research. X.T. developed the models and conducted the simulations. X.T. and F.Y. analyzed the results. X.T., S.D.S., and F.Y. wrote the manuscript. All authors reviewed the final manuscript. **Competing interests:** S.D.S. is a co-founder of Swift Solar Inc. **Data and materials availability:** All data needed to evaluate the conclusions in the paper are present in the paper and/or the Supplementary Materials. Additional data related to this paper may be requested from the authors.

Submitted 23 January 2020

Accepted 19 June 2020

Published 31 July 2020

10.1126/sciadv.abb0055

Citation: X. Tian, S. D. Stranks, F. You, Life cycle energy use and environmental implications of high-performance perovskite tandem solar cells. *Sci. Adv.* **6**, eabb0055 (2020).

Life cycle energy use and environmental implications of high-performance perovskite tandem solar cells

Xueyu Tian, Samuel D. Stranks and Fengqi You

Sci Adv 6 (31), eabb0055.
DOI: 10.1126/sciadv.abb0055

ARTICLE TOOLS	http://advances.sciencemag.org/content/6/31/eabb0055
SUPPLEMENTARY MATERIALS	http://advances.sciencemag.org/content/suppl/2020/07/27/6.31.eabb0055.DC1
REFERENCES	This article cites 49 articles, 2 of which you can access for free http://advances.sciencemag.org/content/6/31/eabb0055#BIBL
PERMISSIONS	http://www.sciencemag.org/help/reprints-and-permissions

Use of this article is subject to the [Terms of Service](#)

Science Advances (ISSN 2375-2548) is published by the American Association for the Advancement of Science, 1200 New York Avenue NW, Washington, DC 20005. The title *Science Advances* is a registered trademark of AAAS.

Copyright © 2020 The Authors, some rights reserved; exclusive licensee American Association for the Advancement of Science. No claim to original U.S. Government Works. Distributed under a Creative Commons Attribution NonCommercial License 4.0 (CC BY-NC).